Activation and Inactivation Kinetics of an E-4031-Sensitive Current from Single Ferret Atrial Myocytes

Shuguang Liu, Randall L. Rasmusson, Donald L. Campbell, Shimin Wang, and Harold C. Strauss
Departments of Medicine, Biomedical Engineering and Pharmacology, Duke University Medical Center, Durham,
North Carolina 27710 USA

ABSTRACT   Ferret atrial myocytes can display an E-4031-sensitive current (I_{Kr}) that is similar to that previously described for guinea pig cardiac myocytes. We examined the ferret atrial I_{Kr} as the E-4031-sensitive component of current using the amphotericin B perforated patch-clamp technique. Steady-state I_{Kr} during depolarizing pulses showed characteristic inward rectification. Activation time constants during a single pulse were voltage dependent, consistent with previous studies. However, for potentials positive to +30 mV, I_{Kr} time course became complex and included a brief transient component. We examined the envelope of tails of the drug-sensitive current for activation in the range −10 to +50 mV and found that the tail currents for I_{Kr} do not activate with the same time course as the current during the depolarizing pulse. The activation time course determined from tail currents was relatively voltage insensitive over the range +30 to +50 mV ($n = 5$), but was voltage sensitive for potentials between −10 and +30 mV and appeared to show some sigmoidicity in this range. These data indicate that activation of I_{Kr} occurs in at least two steps, one voltage sensitive and one voltage insensitive, the latter of which becomes rate limiting at positive potentials. We also examined the rapid time-dependent inactivation process that mediates rectification at positive potentials. The time constants for this process were only weakly voltage dependent over the range of potentials from −50 to +60 mV. From these data we constructed a simple linear four-state model that reproduces the general features of ferret I_{Kr}, including the initial transient at positive potentials and the apparent discrepancy between the currents during the initial depolarizing pulse and the tail current.

INTRODUCTION

Cardiac delayed rectifier K^+ channels have been of long-standing interest because of their importance in repolarization and pacemaker activity (McAllister et al., 1975; Noble, 1984; Shibata and Giles, 1985; DiFrancesco, 1985; Anumonwo et al., 1992; Campbell et al., 1992; Wang et al., 1993; Muraki et al., 1995; Verhiejck, 1995). Multiple delayed rectifier K^+ currents are now recognized to contribute to the cardiac action potential. The number, kinetic description, and pharmacology of these K^+ channels have been extensively investigated (Balser et al., 1990; Sanguinetti and Jurkiewicz, 1991; Apkon and Nerbonne, 1991; Kass, 1995; Wang et al., 1994; Backx and Marban, 1993; Snyders et al., 1993; Beuckelmann et al., 1993). Advances in both experimental techniques and approaches have increased our understanding of these K^+ currents from the early "I_{X1}" and "I_{X2}" formulations of the cardiac delayed rectifier (Noble and Tsien, 1968, 1969; Noble, 1984) to the point where the molecular bases of some individual currents have been, or are being, identified (e.g., Fedida et al., 1993; Sanguinetti et al., 1995). Two distinct types of K^+ channels have been shown to contribute to delayed rectification in cardiac muscle (Sanguinetti and Jurkiewicz, 1990), one slowly activat-

ing (I_{Ks}) and another that activates much more rapidly and shows strong inward rectification (I_{Kr}) (Sanguinetti and Jurkiewicz, 1990; Wang et al., 1994). The I_{Kr} component is selectively blocked by the Class III antiarrhythmic compounds E-4031 (1-[2-(6-methyl-2-pyridyl)ethyl]-4-(4-methylsulfonylaminobenzoyl)piperidine), dofetilide, and almokalant (Carmeliet, 1992, 1993; Jurkiewicz and Sanguinetti, 1993). In addition, I_{Kr} is believed to have h-*erg* (*h*uman *e*ther-à-go-go *r*elated *g*ene) as its molecular basis (Sanguinetti et al., 1995; Trudeau et al., 1995). Furthermore, mutations in this gene have been linked to a familial form of long QT syndrome (Curran et al., 1995). Despite the considerable interest in and investigation of this current, a comprehensive quantitative description of I_{Kr} gating has not yet appeared in the literature. This incomplete description may reflect incompatibilities (Clay et al., 1995) between measured macroscopic kinetics and conventional Hodgkin and Huxley (H-H) (Hodgkin and Huxley, 1952) analysis, particularly with respect to activation. In particular, Clay et al. (1995) have recently noted that the voltage dependence of I_{Kr} activation time constants cannot be reconciled with measured steady-state activation using a first-order H-H gating variable. In addition, the time and voltage dependence of the inactivation/rectification process has not been characterized over the physiological range of potentials. As a result, the contribution of inactivation to rectification of I_{Kr} at depolarized potentials is unknown. To develop a comprehensive mathematical model of I_{Kr} we carried out a non-H-H analysis of the E-4031-sensitive current in isolated ferret right atrial myocytes. Such an approach was necessary to resolve the paradox surrounding I_{Kr} activation and to

provide a framework on which to base structure-function studies of h-*erg*.

The development of our I_{Kr} model required the use of novel voltage-clamp protocols that allowed us to measure the time and voltage dependence of activation at depolarized potentials, where I_{Kr} currents are expected to be negligible because of rectification. We also measured inactivation kinetics in the depolarized range of potentials and the instantaneous *I-V* relationship for this channel. This data was then used to develop a sequential four-state model of channel activation and inactivation that quantitatively reproduces the major features of the E-4031-sensitive current in ferret atrial myocytes. The model can reconcile the apparent paradox between steady-state activation and activation kinetic analysis and demonstrates novel interactions between inactivation and activation.

A preliminary account of this work has appeared in abstract form (Liu et al., 1996)

MATERIALS AND METHODS

Myocyte isolation

Single myocytes were isolated from the right atria of 10–16-week-old ferrets (Marshall Farms, North Rose, NY) via the Langendorff perfusion method. Animals were anesthetized by intraperitoneal injection of sodium pentobarbital (50–75 mg), and the hearts were rapidly excised and mounted on a perfusion apparatus as previously described (Campbell et al., 1993). All solutions were maintained at 37°C. The initial perfusion (5–10 min) was with control saline containing (mM): 144 NaCl, 5.4 KCl, 1 MgCl$_2$, 1.8 CaCl$_2$, 10 HEPES, pH 7.25. The heart was then perfused for 5 min with a nominally Ca^{2+}-free 100 μM EGTA solution (same as control except that CaCl$_2$ was removed, MgCl$_2$ was increased to 3.5 mM, 20 mM taurine, 10 mM creatine added). This was then followed by a 12–25-min perfusion with a 100 μM CaCl$_2$ solution (EGTA removed) containing 1 mg/ml collagenase (Type II; Worthington, Freehold, NJ), 0.2 mg/ml protease (Type XIV; Sigma, St. Louis, MO), and 0.05 mg/ml elastase (Type II-A; Sigma). The right atrium was then dissected free, placed in a 15-ml centrifuge tube containing fresh enzyme solution with an additional 10 mg/ml bovine serum albumin (essentially fatty acid free; Sigma), and gently shaken (~1–2/s) on a rocker table placed in an incubator at 37°C. Myocytes were harvested at 10-min intervals and stored at room temperature in saline solution (mM): 144 NaCl, 5.4 KCl, 1 MgSO$_4$, 1.8 CaCl$_2$, and 10 HEPES, pH 7.4. All experiments were performed within 5–7 h of isolation.

Electrophysiological techniques

In all experiments myocytes were voltage clamped using the amphotericin-permeabilized patch-clamp technique. The patch-clamp amplifier was an Axopatch 1-D (Axon Instruments, Foster City, CA). Voltage-clamp protocols were generated using PClamp 5.5 software. Patch-clamp electrodes (1.5 mm o.d. borosilicate tubing, TW150F-4; WP Instruments) were pulled and gently heat polished to a tip diameter of approximately 1 μm as previously described (Campbell et al., 1993). The electrode tips were backfilled with amphotericin B-containing solution (120 K-methane sulfonate, 20 KCl, 10 HEPES, 240 μg amphotericin B/ml, pH 7.40). Aliquots of myocytes were pipetted into a small (0.5 ml) recording chamber mounted on the modified stage of an inverted Nikon Diaphot microscope, and after settling, the myocytes were continuously superfused (1–4 ml/min) with a gravity feed system. Details concerning the recording chamber and grounding apparatus were as previously described (Campbell et al., 1993). After gigaseal formation the reduction in access resistance was

monitored until it reached steady-state values (5–15 MΩ), which usually occurred within 40 min. All experiments were conducted at room temperature (22–24°C) to resolve inactivation kinetics that would be too fast to resolve at 37°C (Sanguinetti et al., 1995).

Solutions and drugs

Extracellular solution contained (mM): 144 *N*-methyl-D-glucamine Cl, 5.4 KCl, 3.0 MgCl$_2$, 10 HEPES, pH 7.40. E-4031 was generously provided by Esai Co., Tsukuba Research Laboratories, Japan. Unless otherwise noted, all currents shown are drug-sensitive difference currents. I_{Kr} was defined to be the drug-sensitive current.

Data analysis

Data were filtered at 2 kHz, digitized, and analyzed directly using pClamp software (Axon Instruments). Averaged activation data were fit to a sequential three-state activation model using custom programs written in Borland C++ implementing a Marquardt optimization procedure similar to that described previously for optimizing a model of I_{to} activation to average data (Campbell et al., 1993). Model simulations were calculated using a fourth-order Runge-Kutta algorithm with a variable step size as previously described (Campbell et al., 1993) and implemented in Borland C++. Numerical accuracy was confirmed by demonstrating insensitivity to step size.

RESULTS

General characteristics

To isolate I_{Kr} from as many overlapping currents as possible before drug subtraction, we used a combination of ionic substitution and voltage-clamp protocols. We employed the pulse protocol described in Fig. 1 in the absence (Fig. 1 *A*) and presence (Fig. 1 *B*) of 1 μM E-4031 with 0 Na$^+$ and nominally Ca^{2+}-free extracellular solution to isolate I_{Kr} from other non-K$^+$ currents. In addition, cells were held at -40 mV to inactivate I_{to} and any residual Na$^+$ or Ca^{2+} currents and pulsed to positive potentials for 1000 ms to activate I_{Kr}. Only those currents elicited by pulses between -30 and 0 mV are shown in Fig. 1, *A–C*. Fig. 1 *C* shows the drug-sensitive currents obtained by subtracting the records in Fig. 1 *B* from Fig. 1 *A*. Note that the tail currents generated on repolarization back to -40 mV (Fig. 1 *A*) are essentially eliminated by 1 μM E-4031 (Fig. 1 *B*). The steady-state *I-V* relationship (Fig. 1 *D*) shows the characteristic inward rectification described previously for I_{Kr} in isolated guinea pig ventricular myocytes (Sanguinetti and Jurkiewicz, 1990).

To determine the sensitivity of I_{Kr} to E-4031, we determined its dose-response relationship from an analysis of drug effects on the tail currents at -40 mV. Block of I_{Kr} was taken as the fractional decrease in P2 tail current. The raw data in Fig. 2 *A* show the currents before application of E-4031, in the presence of 0.2 μM E-4031 and after 30 min of washout in control solution (P1 = $+10$ mV). In contrast to earlier reports on the effects of E-4031 on guinea pig ventricular myocytes (Sanguinetti and Jurkiewicz, 1990), block of the deactivation tail currents was fully reversible. This difference in reversiblility may reflect a difference in

FIGURE 1 I_{Kr} current in ferret right atrial myocytes. (A) Raw currents recorded in control saline (Na^+ free, nominally 0 Ca^{2+}; see Materials and Methods). Cells were held at -40 mV, depolarized from -30 to 0 mV in 10-mV steps for 1 s, and returned to a holding potential of -40 mV. (B) Currents recorded from the same cell as in A, but in the presence of 1 μM E-4031. Note that the tail currents were essentially eliminated by E-4031. (C) E-4031-sensitive currents obtained by subtraction of current traces in B from those in A. Solid lines during depolarization represent fitting of single exponentials to individual current traces (time constants of 980, 748, 578, and 268 ms for potentials of -30, -20, -10, and 0 mV, respectively). (D) Isochronal current-voltage relation during depolarization. Currents were measured at the end of 1-s depolarizing pulses and plotted against the potentials at which currents were measured. Note the characteristic inward rectification typical of I_{Kr} (data plotted as mean $\pm$ SE, $n = 7$; straight line indicates zero current measured at -80 mV).
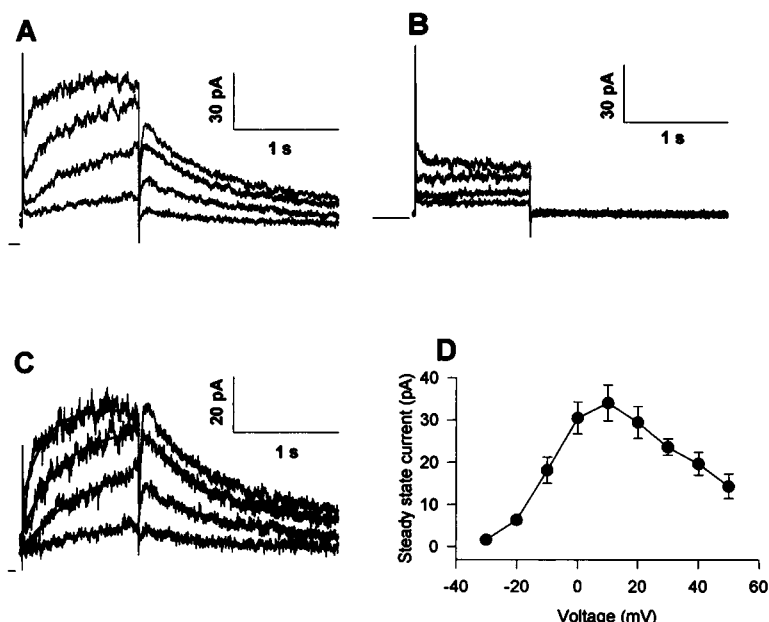
species or a difference in voltage-clamp protocol employed (see Discussion). The average dose-response curve for E-4031 indicates an EC_{50} of 10.3 nM (Fig. 2 B).

Activation

The tail currents upon repolarization to -40 mV were also analyzed to determine the steady-state activation characteristics. Peak P2 currents similar to those in Fig. 1 C were normalized to those obtained for a P1 potential of $+50$ mV and plotted as a function of P1 potential to obtain the steady-state activation curve shown in Fig. 3 A. Steady-state activation was well described by a Boltzmann function with $V_{1/2} = -13.0$ mV and $k = 8.4$ mV. Single exponential fits to the time course of activation of the drug-sensitive outward currents in response to the initial depolarization were analyzed (e.g., Fig. 1 A) to provide a first approximation to the activation process. When analyzed in this fashion, apparent activation rate showed a strong voltage dependence (Fig. 3 B). The time-constant data in Figs. 1 and 3 B are presented for comparison with previous studies and are not used for model development.

Because of the inward rectification, the E-4031-sensitive currents at positive potentials were small. Therefore, direct fitting of currents during a single depolarizing pulse was abandoned in favor of an alternative fitting procedure to determine the time course of activation. Fig. 4 A shows typical current records obtained using this procedure. Briefly, the myocytes were depolarized to the activation potential (P1 $= +20$ mV) for varying durations of time (Δt). Upon repolarization to -40 mV, a tail current was recorded, the peak amplitude of which was plotted as a function of Δt (Fig. 4 B). Repeating this protocol for test potentials of -10 to $+50$ mV in 10-mV steps gave an accurate reconstruction of the time and voltage dependence of activation. Because

the tail currents at -40 mV were demonstrated to consist entirely of I_{Kr}, we analyzed the unsubtracted tail currents directly. A limited analysis of the activation of drug-sensitive tail currents demonstrated no significant differences from the unsubtracted records (data not shown).

Two differences between the direct-fit analysis and the tail current analysis were apparent: 1) the time course of activation of the tail currents was slower at depolarized potentials than that of the drug-sensitive currents measured during the initial depolarizing pulse; and 2) the time course of activation of the tail currents became voltage insensitive in the range of $+30$ to $+50$ mV. The saturation of rate of activation as a function of voltage was particularly significant, because this indicated that a voltage-insensitive step became rate limiting in the activation pathway. Therefore, at a minimum, the activation process must involve at least one voltage-sensitive and one voltage-insensitive step. The order of these processes can occur in two ways:

$$ \overset{i}{C} \rightleftarrows \overset{v}{C} \rightleftarrows O $$

Model 1

$$ \overset{v}{C} \rightleftarrows \overset{i}{C} \rightleftarrows O $$
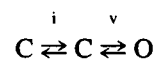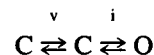
Model 2

where C denotes closed states, O denotes the open state, and v and i denote voltage-sensitive and voltage-insensitive steps, respectively. The order of these transitions cannot be determined from the time and voltage dependence of the activation data (Hille, 1992). However, the presence or absence of voltage dependence of the kinetics of deactivation of the drug-sensitive tail currents can indicate whether
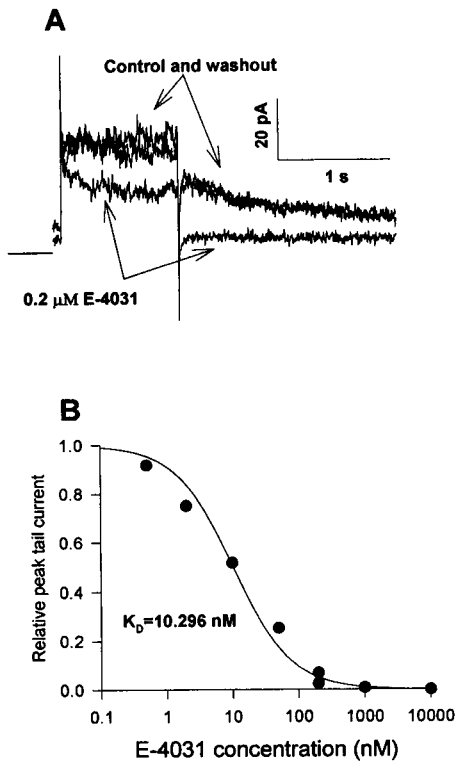
A

Control and washout

0.2 µM E-4031

B

$K_D = 10.296$ nM

E-4031 concentration (nM)

FIGURE 2   Dose-response relationship of I_{Kr} for E-4031 determined from tail current analysis in isolated ferret atrial myocytes. (A) Cells were held at −40 mV, depolarized to +10 mV for 1 s, and hyperpolarized to −40 mV. Tail current was totally blocked by 0.2 µM E-4031. Note the slight decrease in holding current in the presence of E-4031, reflecting blockade of partially activated channels at −40 mV. Complete recovery of the blocked current was achieved after extended washout for 30 min (straight line indicates zero current measured at −80 mV). (B) Average dose-response curve of ferret I_{Kr} for E-4031. Data were pooled from four experiments. Solid curve represents fitting of the data to equation $I_{tail}/I_{tail,\ control} = K_D/(K_D + [\text{E-4031}])$, with a K_D of 10.3 nM.

a voltage-sensitive or -insensitive step immediately precedes channel opening.

We measured the time constants of deactivation of the drug-sensitive tail currents using a two-pulse protocol (Fig. 5). Myocytes were clamped from a holding potential of −40 mV to a P1 potential of +20 mV for 1 s to fully activate the current. P1 was then followed by a P2 pulse to various potentials (−120 to −20 mV in 10-mV increments). In Fig. 5 only the last 50 ms of the P1 pulse is shown, to more clearly display the tail currents. After repolarization to negative potentials there is a clear delay or "hook" visible in the tail currents. Such a "hook" is indicative of rapid recovery from inactivation/rectification followed by a slower decay of the current due to deactivation. However, we did not analyze the rapid recovery from inactivation in these experiments. We did analyze the slow time constants of deactivation, however, as shown in Fig. 5. Clearly, the deactivation time constants are strongly voltage dependent, indicating that the voltage-dependent step communicates directly with the open state. Therefore, we adopted Model 1
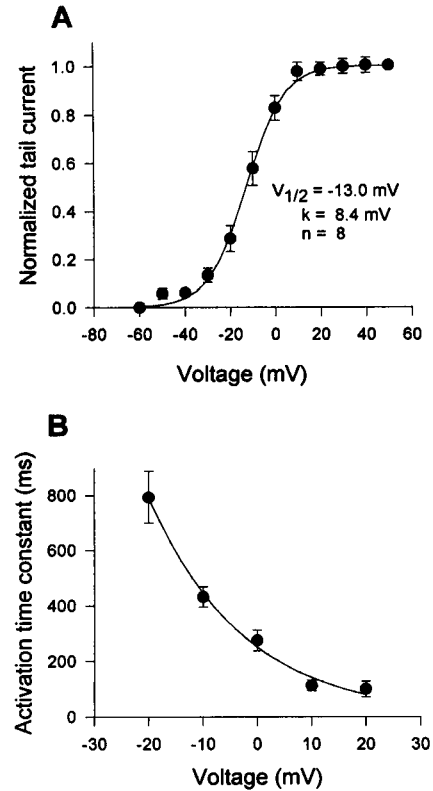
A

$V_{1/2} = -13.0$ mV
$k = 8.4$ mV
$n = 8$

Voltage (mV)

B

Voltage (mV)

FIGURE 3   Kinetic properties of activation during a single depolarizing pulse. (A) Steady-state activation of I_{Kr}. The protocol described in Fig. 1 was applied to evoke tail currents. Peak tail currents measured upon repolarization to −40 mV were normalized to those measured for a pulse to +50 mV and plotted against pulse potential. Fitting of the data ($n = 8$) to a Boltzmann equation $I_{normalized} = 1/(1 + \exp(-(V_m - V_{1/2})/k))$ generated the solid curve with a slope factor $k = 8.4$ mV and $V_{1/2} = -13.0$ mV. (B) Voltage dependence of apparent activation time constants determined using direct-fit analysis. Activation time courses were fit to a single exponential equation, and the resultant average time constants ($n = 9$) were plotted against activation potentials. The averaged apparent time constants showed an exponential dependence on membrane potential, as shown by the smooth curve time constant curve, $\tau_a = 1/(A\ \exp(BV_m))$ where $A = 0.00399$/ms and $B = 0.0575$/mV.

and applied automated parameter identification to fit the average activation time course data, average steady-state activation, and deactivation rate constant data simultaneously (Fig. 6, A–C). A comparison of the model results using the optimized model parameters with the experimental data is shown in Fig. 6; it demonstrates that Model 1 is capable of quantitatively reproducing the experimental results.

Inactivation/rectification

As previously noted in Fig. 5, the initial time-dependent component or "hook" preceding deactivation has been interpreted to reflect a time-dependent recovery from an inactivation-like process that produces the rectifying properties of I_{Kr} (Shibasaki, 1987; Sanguinetti et al., 1995). However, the time and voltage dependence of this process
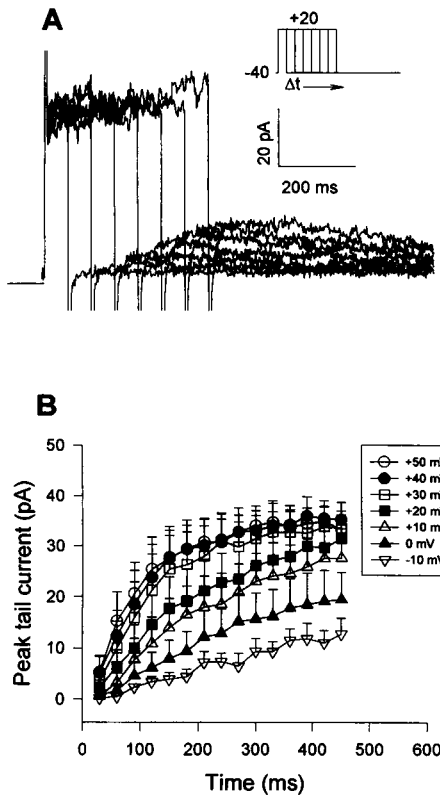
A

B

A

B

FIGURE 4 Activation time course estimated using tail current measurements. (A) Representative tail currents were elicited by depolarizations to +20 mV from a holding potential of −40 mV using different P1 durations. Experiments were performed in control saline without E-4031 subtraction (straight line indicates zero current measured at −80 mV). (B) Average activation time course of peak tail currents obtained for pulses to varying potentials. Cells were held at −40 mV and then stepped to a P1 potential (−10 to +50 mV) for varying periods of time before repolarization to −40 mV. Currents were measured as peak currents during repolarization to −40 mV (data plotted as mean ±SE, n = 4).
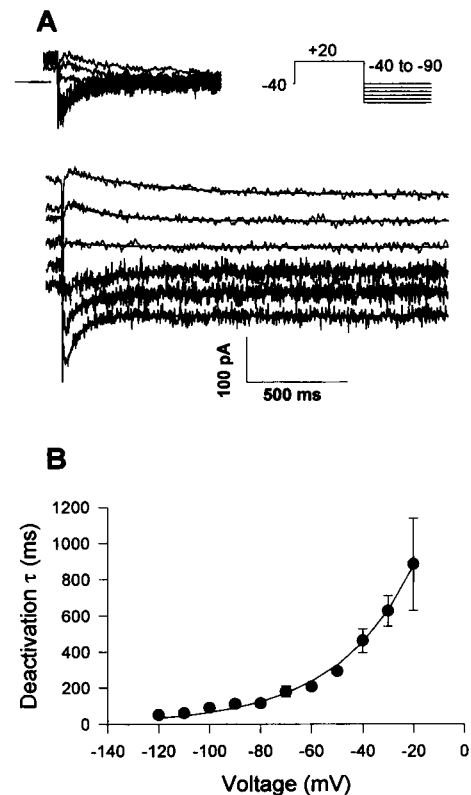
FIGURE 5 Deactivation time course. (A) Raw current traces. Holding potential was −40 mV. A depolarizing prepulse to +20 mV of 1 s duration was delivered to the myocytes before subsequently stepping to various potentials. This prepulse was truncated to better display the deactivation tail currents. Currents were offset to separate them for display purposes. Currents without offset are shown as an inset (straight line indicates zero current measured at −80 mV). Solid curves are single exponential fits to current traces at potentials of −40, −50, −60, −70, −80, and −90 mV, with time constants of 429, 239, 212, 163, 107, and 63 ms, respectively. A variety of factors may have contributed to increased noise at hyperpolarized potentials. First, these drug-subtracted records can remove the systematic components of other currents, but will not eliminate the intrinsic noise resulting from the random opening and closing of other channels that are active in this voltage range, e.g., I_{K1}. In addition, we cannot rule out increased noise due to deterioration of the gigaseal during the course of the experiment, although no increase in leak current was observed. (B) Average voltage dependence of deactivation time constants. Averaged time constants from seven experiments were plotted against deactivation potentials. Fitting the data to the equation, $\tau_d = 1/(A \exp(BV_m))$ yielded an A of 0.000593 ms^{-1} and a B of −0.0328 mV^{-1}.

has not been studied in the positive potential range. Furthermore, the instantaneous current-voltage relationship for I_{Kr} has not been established. To quantitate the instantaneous current-voltage relationship and the time and voltage dependence of the inactivation/rectification process, we employed a three-pulse voltage-clamp protocol (Fig. 7 A). A P1 pulse to +50 mV was initially applied for 600 ms to fully activate I_{Kr}, which was followed by a P2 pulse to −40 mV for 50 ms to remove inactivation without allowing sufficient time for deactivation to occur. A final P3 pulse was then applied to different potentials from −90 to +50 mV. Typical traces using this protocol are shown in Fig. 7 A. The P1 pulse was truncated to more clearly display the rapid inactivation process during the P3 pulse.

The instantaneous I-V relationship was derived by measuring an isochronal point 3 ms after the onset of the pulse. This small delay allowed separation of the ionic current from any residual uncompensated capacitance current and the associated membrane potential rise time without allowing significant change in the inactivation of I_{Kr}. The average

instantaneous I-V relationship for the channel is shown in Fig. 8 A. The relationship was linear with a conductance of 2.16 nS/cell (35.4 ± 4.6 pF/cell, n = 6). The linearity of the instantaneous I-V relationship indicates that inactivation is responsible for the inward rectification of steady-state I_{Kr}. Fig. 8 B shows the steady-state inactivation relationship, calculated as the ratio of the currents measured 100 ms after the beginning of P3 to the instantaneous currents measured at the beginning of P3. This measurement estimated inactivation relative to the degree of steady-state inactivation at −40 mV. The absolute value of steady-state inactivation was obtained by estimating the degree of steady-state inac-
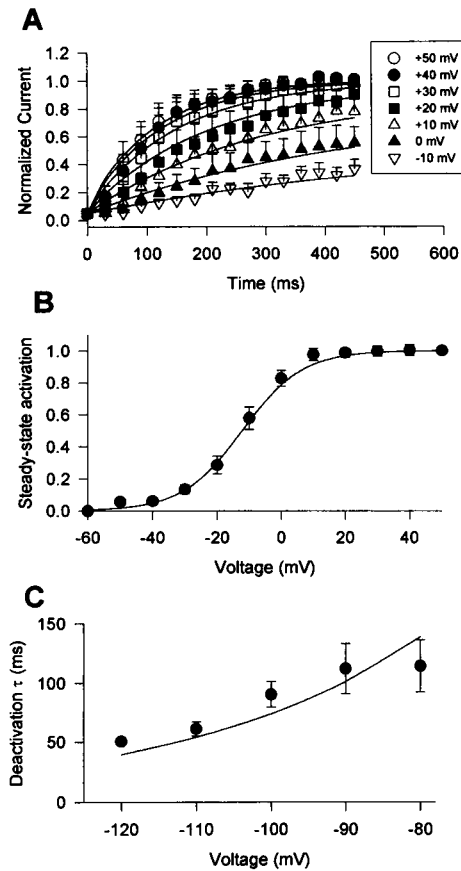
A

B

C

FIGURE 6 Simultaneous fitting of the two transition Model 1 to the average activation data. (A) Fit (solid curve) to activation time course. (B) Fit to steady-state activation. (C) Fit to deactivation time constants. Data from all three panels were used simultaneously during optimization to constrain model parameters. Symbols represent averaged experimental data. Solid lines are fitting results. For activation time course and steady-state activation, the fitting procedure optimized an implementation of the linear three-state model, where k_f and k_b were the voltage-independent rate constants that governed the C_0 to C_1 and C_1 to C_0 transitions, respectively; $\alpha_a(V_m)$ and $\beta_a(V_m)$ are the voltage-dependent rate constants for the C_1 to O and O to C_1 transitions, where the forms of the equations are $\alpha_a(V_m) = A_1$ $\exp(B_1 V_m)$ and $\beta_a(V_m) = A_2 \exp(B_2 V_m)$. k_f, k_b, A_1, A_2, B_1, and B_2 were the free parameters that were optimized. The activation time course estimated from normalization of the tail current data from Fig. 4 B, steady-state activation data from Fig. 3 A, and deactivation data from Fig. 5 B were fit with a customized program to a calculated solution of activation time course, with the calculated steady-state activation by a simulation protocol designed to match the one employed experimentally in Fig. 3 A. The deactivation time constant at hyperpolarized potentials was assumed to be equal to $1/\beta_a(V_m)$, where $\beta_a(V_m)$ is the voltage-dependent backwards rate constant governing the transition from O to C_1. Only data points equal to or more negative than -80 mV were used to avoid contamination of data from the inactivation process. Fitting yielded the following activation parameters: $k_f = 0.00976$ ms^{-1}, $k_b = 0.190$ ms^{-1}, $A_1 = 0.0438$ ms^{-1}, A_2 $= 0.0755$ ms^{-1}, $B_1 = 0.000583$ mV^{-1}, and $B_2 = -0.0315$ mV^{-1}.

tivation at -40 mV from the relief of inactivation at -90 mV, as indicated in the legend of Fig. 8. The solid line in Fig. 8 B represents a model fit of the final model inactivation rate constants to the steady-state inactivation relation. These rate constants were also simultaneously fit to the time constant data for inactivation as described below.
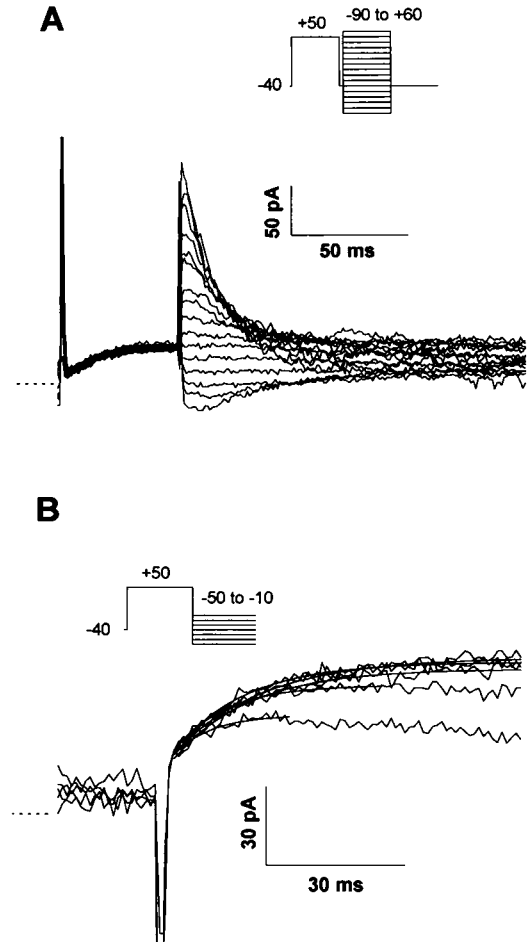
A

B

FIGURE 7 Inactivation and its recovery. (A) Development of inactivation at positive potentials. A preconditioning P1 pulse of $+50$ mV with 500 ms duration was applied (data truncated to more clearly display rapid inactivation) to cells before they were clamped back to -40 mV for 50 ms (P2) to allow removal of inactivation. Fifty milliseconds was determined to be the peak of the deactivation tail currents at -40 mV. A final P3 pulse to potentials ranging between -90 and $+60$ mV was applied to allow examination of the instantaneous current and the rapid re-establishment of inactivation. (B) Recovery from inactivation. A preconditioning pulse to $+50$ mV was applied for 500 ms to allow the current to fully activate and inactivate. Recovery was observed as the time-dependent initial increase in current at potentials varying between -10 and -50 mV. Solid lines are the single exponential fits to the rising phase of the current from the end of the capacitive transient to the peaks of tail currents, giving time constant recovery from inactivation of 16.4, 19.3, 15.4, 11.2, and 8.2 ms for -10, -20, -30, -40, and -50 mV, respectively. The dashed line indicates zero current measured at -80 mV and that the early portions of the current traces have been truncated.

The time course of inactivation during the P3 pulse described above was fit with a single exponential and yielded an estimate of the rate of inactivation at positive potentials. The average data from this fitting procedure are shown by the filled circles in Fig. 8 C. To estimate the time constants of recovery from inactivation, a double pulse protocol similar to those used previously to characterize the kinetics of recovery from inactivation of h-*erg* (Sanguinetti et al., 1995) was used (Fig. 7 B). Myocytes were stepped
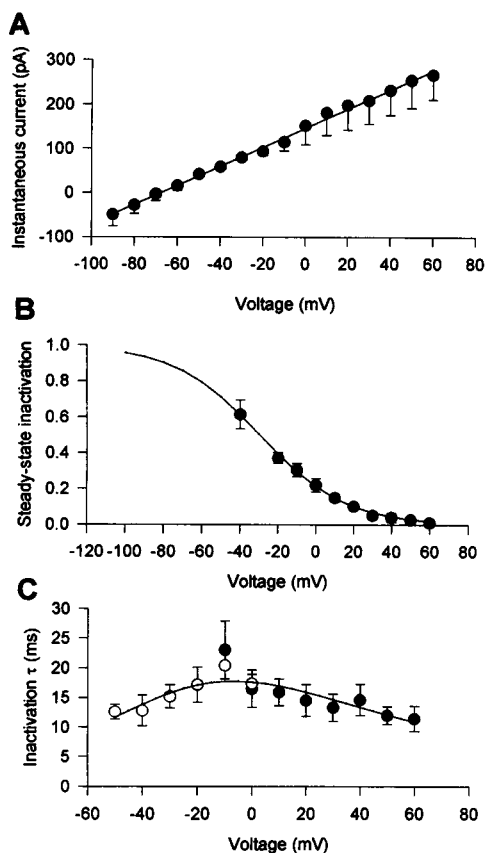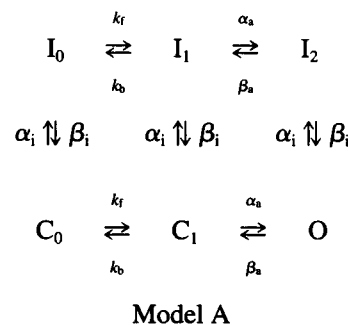
A

B

C

FIGURE 8 Inactivation/rectification properties of I_{Kr}. (A) Instantaneous current-voltage relation. Instantaneous currents were measured at the beginning of the P3 pulse, as described in Fig. 7 A. The straight line is a linear regression to the averaged data ($I_{instantaneous} = 2.16V_m + 145.7$) and yielded a reversal potential of -67.5 mV (a value similar to that reported for I_{Kr} in rabbit ventricular myocytes; Clay et al., 1995). Note that the instantaneous current is linear, indicating that inward rectification is entirely due to the time-dependent inactivation process. (B) Steady-state inactivation. Steady-state inactivation relative to the degree of inactivation at -40 mV was calculated as the ratio of currents measured 100 ms after the onset of the P3 pulse (see Fig. 7) to the instantaneous currents measured at the same potentials. The resulting ratios were then normalized to the degree of inactivation at -40 mV, which was measured as the time-dependent increase in current relative to that occurring at -90 mV during the P3 pulse. Solid lines result from a simultaneous fitting of $\alpha_i(V_m)$ and $\beta_i(V_m)$, ($Inact_{ss} = 1/(1 + \alpha_i(V_m)/\beta_i(V_m))$) to this data and the data in C. (C) Voltage dependence of inactivation time constants. Empty circles are time constants for recovery from inactivation (Fig. 7 B). Filled circles are inactivation time constants obtained by fitting single exponentials to current traces described in Fig. 7 A. Data shown are mean ± SE ($n = 6$). The smooth line represents the results of simultaneous fitting of $\alpha_i(V_m)$ and $\beta_i(V_m)$, where $\tau_i = 1/(\alpha_i(V_m) + \beta_i(V_m))$ and $\alpha_i(V_m) = A_3 \exp(A_4 V_m)$ and $\beta_i(v) = B_3 \exp(B_4 V_m)$. The optimal parameter values were $A_3 = 0.00446$ ms^{-1}, $A_4 = 0.0117$ mV^{-1}, $B_3 = 0.0121$ ms^{-1}, and $B_4 = -0.0324$ mV^{-1}.

from a holding potential of -40 mV to a P1 potential of $+40$ mV for 500 ms to fully activate and then inactivate the current. This was followed by a P2 pulse of different amplitudes (-10 to -50 mV in 10-mV increments). The initial increase in tail current during P2 was fit to an exponential starting 5 ms after the onset of the pulse. The average time constants for recovery from inactivation are plotted in Fig.
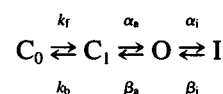
8 C (*empty circles*). Voltage-dependent rate constants were calculated by simultaneously fitting the steady-state data in Fig. 8 B and the kinetic data in Fig. 8 C. Both the steady-state and kinetic data were well described by a single pair of H-H-like rate constants, shown as the solid line in Fig. 8, B and C.

Modeling

A complete model describing I_{Kr} involved incorporation of inactivation into Model 1. We considered two alternative formulations for inactivation. The first formulation considered inactivation to be independent of activation in a fashion similar to that originally proposed by H-H, and is shown as model A:

$$I_0 \underset{k_b}{\overset{k_f}{\rightleftarrows}} I_1 \underset{\beta_a}{\overset{\alpha_a}{\rightleftarrows}} I_2$$

$$\alpha_i \updownarrow \beta_i \qquad \alpha_i \updownarrow \beta_i \qquad \alpha_i \updownarrow \beta_i$$

$$C_0 \underset{k_b}{\overset{k_f}{\rightleftarrows}} C_1 \underset{\beta_a}{\overset{\alpha_a}{\rightleftarrows}} O$$

Model A

where α_i and β_i are the voltage-dependent rate constants for inactivation as described in Fig. 8. The second formulation considered inactivation to be coupled to activation in a fashion similar to the "ball and chain" model recently proposed for other inactivating K$^+$ channels (e.g., Hoshi et al., 1990) and similar to that used to describe open channel block by intracellular blocking compounds (e.g., Armstrong, 1966). This coupled model of ferret I_{Kr} is shown as model B:

$$C_0 \underset{k_b}{\overset{k_f}{\rightleftarrows}} C_1 \underset{\beta_a}{\overset{\alpha_a}{\rightleftarrows}} O \underset{\beta_i}{\overset{\alpha_i}{\rightleftarrows}} I$$

Model B

Models A and B were used to simulate activation experiments, in which cells were depolarized from a holding potential of -40 mV to different potentials for a duration of 1 s. Results from these simulations are shown in Fig. 9. There were significant differences between the simulations of the two models. In particular, model A predicts a very small, rapid transient at positive potentials, due to rapid time-dependent inactivation of those channels that activate relatively rapidly from the C_1 or O state at -40 mV. Model A also predicts a weak voltage dependence of the time course of activation, with saturation in the rate of outward current activation becoming apparent at positive potentials. Model B predicts an apparent activation time course that is strongly voltage dependent at potentials of $+20$ mV or less. At potentials positive to $+20$ mV the predicted current begins to display a relatively slowly inactivating transient
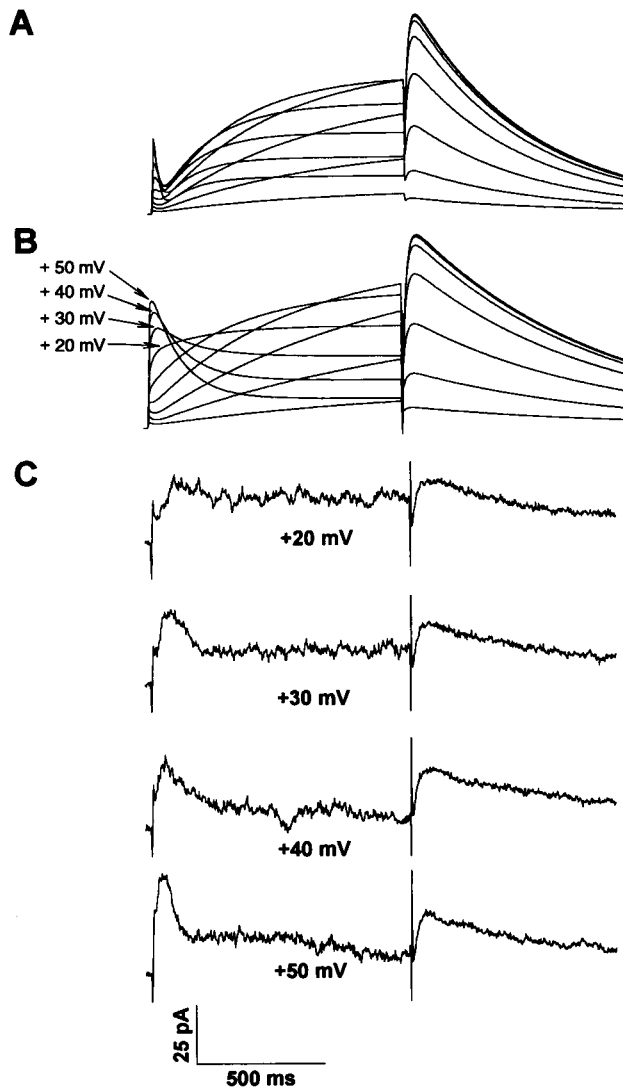
FIGURE 9 Comparison of simulated I_{Kr} activation current with that recorded from cells. The simulated voltage-clamp protocol was identical to that applied to the experimental examples shown in C. (A) Simulation of model A described in the text. The transient current is much smaller and faster than that predicted from model B and activation rate at lower potentials had a weak slow voltage dependence. (B) Simulation of model B as described in the text, using the experimentally determined activation and inactivation parameters. Note the appearance of a large, relatively slowly inactivating transient at potentials more positive than +20 mV. (C) Experimentally recorded E-4031-sensitive currents. Holding potential was −40 mV. The myocytes were depolarized for 1 s to potentials from +20 to +50 mV and repolarized back to −40 mV. Note that the magnitude and time dependence of the initial transient in the E-4031 sensitive current closely resemble model B (A) but appear to be inconsistent with model A (B).

component. This transient component does not arise from the conventional slow inactivation after fast activation but is rather a result of slow delivery of channels to the open state, a situation somewhat analogous to the described behavior of some Na^+ channels at intermediate potentials (Aldrich et al., 1983; Aldrich and Stevens, 1987; see Hille, 1992, for discussion). This transient component should be readily

observable experimentally, and the data in Fig. 9 C show that for potentials positive to +20 mV an E-4031-sensitive transient current was observed. Please note that the current traces shown in Figs. 1, 2, 4, 5, and 7 displayed currents at times and in voltage ranges for which this peak was neither predicted nor observed. This experimentally obtained transient was consistent with that predicted by model B but was inconsistent with model A. It is important to note that at no time in model construction was there any attempt to fit this transient component, i.e., the transient component is a prediction based on model parameters obtained entirely independently of any attempt to "fit" this transient. We therefore conclude that inactivation of ferret I_{Kr} is most likely coupled to activation.

In summary, activation of ferret I_{Kr} requires at least two steps, one voltage sensitive and one voltage insensitive. Rectification results from a time-dependent inactivation-like process that can be modeled as being obligatorily coupled to activation. The resultant four-state linear gating scheme (model B) can reproduce the general behavior of ferret I_{Kr}, as shown in Fig. 10. Fig. 10 A shows the measured response of drug-sensitive currents to a series of three depolarizations. The P1 depolarization (+50 mV, 600 ms) was followed by a 50-ms P2 pulse to −40 mV and in turn by a 600-ms P3 pulse to different potentials (−80 to +60 mV in 10-mV steps) before returning to the holding potential at −40 mV. The model-generated currents from an identical protocol are shown as the traces in Fig. 10 B. These traces show the striking similarities between the I_{Kr} currents recorded under experimental conditions and those generated by the model. The model explains the transient component in the initial depolarization to +50 mV, the removal of inactivation during the subsequent pulse to −40 mV, and the rapid voltage-dependent redevelopment of inactivation, and during the return to rest, the slow deactivation behavior of the channel. In conclusion, a linear four-state model of I_{Kr} is able to reproduce all of the major features of the E-4031-sensitive currents in ferret atrial cells.

DISCUSSION

This paper describes a novel analysis of the activation and inactivation/rectification process of the E-4031-sensitive current (I_{Kr}) in isolated ferret atrial myocytes. Partial kinetic descriptions of this current have appeared before (Shibasaki, 1987; Sanguinetti and Jurkiewicz, 1990), but as noted by Clay et al. (1995), a substantial paradox exists in the literature between measured steady-state activation characteristics and rate constant data. Briefly, Clay et al. (1995) noted that the voltage for the peak of the time constant curve and its general shape, determined from direct fitting of the currents activated in response to a single depolarizing pulse, could not be reconciled with the more depolarized experimentally determined steady-state activation relationship. A similar analysis of our data (see Figs. 1 and 2) would have resulted in the same paradox.
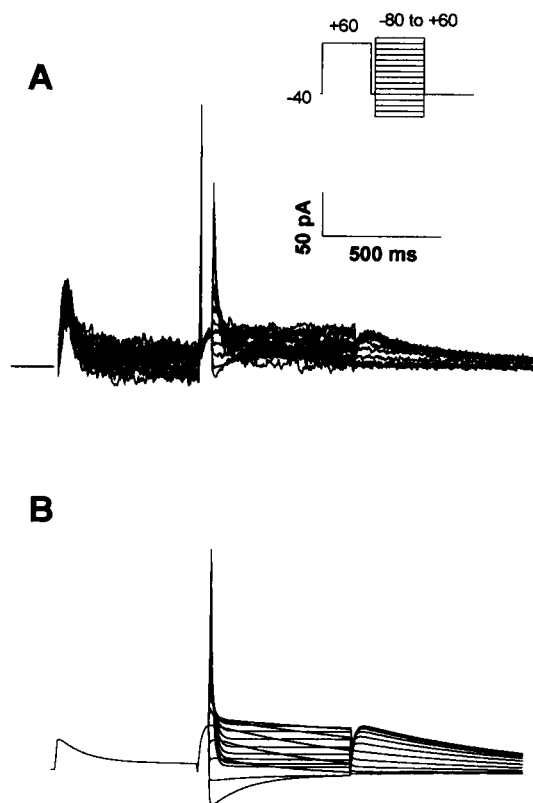
FIGURE 10 Comparison of simulated and experimental I_{Kr} inactivation. (A) Representative experimental data. The cell was held at -40 mV, depolarized to $+50$ mV for 600 ms, clamped to -40 mV for 50 ms, stepped to various potentials (-90 to $+60$ mV in 10-mV steps, for 600 ms), and finally repolarized to -40 mV (straight line indicates zero current measured at -80 mV). (B) Current simulations using model B and the same voltage-clamp protocol as described for A. Note how the model reproduces all of the major features of the E-4031-sensitive current, namely initial transient, relief of inactivation at -40 mV, linear instantaneous current, rapid inactivation, and slow deactivation, which becomes voltage dependent at hyperpolarized potentials.

Activation

Resolution of this activation gating model paradox required the use of different protocols to elucidate the mechanism of activation and to separate it from overlapping processes, in this case rapid inactivation. Rapid inactivation can increase the apparent rate of activation, if it has kinetics that are similar to, or faster than, activation. This process has been suggested to account for the action of the $Kv\beta3$ subunit on the time course of macroscopic current activation of $Kv1.4$ channels at intermediate potentials (Castellino et al., 1995). For I_{Kr}, where rectification arises from a rapid inactivation process, quantitative analysis of activation is critically dependent upon separation of activation from inactivation. By examining the development of the deactivation tail currents, inactivation was eliminated as a factor in this analysis. This occurred because inactivation under these conditions (-40 mV) was largely a steady-state process, due to its more rapid kinetics compared with deactivation. When activation was measured in this fashion, previously unmeasured prop-

erties of I_{Kr} activation became readily apparent. The most important of these was the observation that activation showed substantial sigmoid deviation from single exponential activation and voltage-dependent saturation in its on rate.

The activation process of I_{Kr} therefore is unique among voltage-gated K^+ channels. Although previous studies in *Shaker* K^+ channels have shown that activation occurs through a series of relatively uniformly distributed voltage-sensitive steps, I_{Kr} activation clearly has at least one major voltage-insensitive step. In contrast to some models proposed for other voltage-gated K^+ channels (e.g., Zaggotta and Aldrich, 1990), this voltage-insensitive step is not the final step before opening, but occurs earlier than the final transition. The two-state activation model presented here contains a minimum number of states. However, in Fig. 6 there is a small deviation between the model and the data at early time points (between 0 and 50 ms) at very positive potentials. This deviation suggests some additional delay, possibly due to additional closed states in the activation pathway. In addition, the holding potential used (-40 mV) in these experiments was very close to the threshold for activation of I_{Kr}. In fact, the model predicts that approximately 5% of the total current will be activated at this holding potential. This is consistent with the experimental observation of a small reversible decrease in the holding current when E-4031 is applied (see Fig. 2 A). We cannot rule out the possibility of additional sigmoidicity when the membrane is held at more hyperpolarized potentials (i.e., a "Cole-Moore shift"; Cole and Moore, 1960).

The presence of multiple states in the activation pathway of I_{Kr} is similar to the previously described activation process of other voltage-gated K^+ channels, in that activation occurs with a sigmoid delay. However, the presence of a major rate-limiting voltage-independent step preceding inactivation is unique among voltage-gated K^+ channels. The positively charged residues are well conserved through most of the S4 region in voltage-gated K^+ channels. However, near the end of the cytoplasmic side of S4 in h-*erg* there is one charge reversal at position 540 and additional positive charges at positions 538 and 541. In addition, there is an aspartate residue at position 544. Potentially, the proximity of these charged residues may result in local neutralization of some of the voltage sensor through salt bridge formation. Such interactions could potentially reduce the voltage sensitivity of some activation transitions involving the S4 voltage sensor of h-*erg*. However, it is also possible that lipophilic or allosteric mechanisms are responsible for the voltage-insensitive step in I_{Kr} activation.

Inactivation

Rectification is an important property of I_{Kr} currents and has been attributed to a rapid inactivation-like process. Recovery from this inactivation process has been previously observed as the rapid increase of current, which occurs before

the peak of deactivation tail current records from experiments on I_{Kr} and h-*erg* (Shibasaki, 1987; Sanguinetti et al., 1995). The kinetics of this putative inactivation process were therefore only measured as the "off" (or recovery) rate during tail currents. Therefore, this is the first study to include characterization of both the "off" rate at negative potentials and the on rate at depolarized potentials. The time dependence of this inactivation process could be described by a classical bell-shaped curve (Fig. 8 *C*) and, in contrast to activation, could be quantitatively described by simple first-order voltage-dependent rate constants. In this respect our final model of voltage-dependent inactivation of I_{Kr} is similar to those previously proposed for I_{Kr} and h-*erg*, although it was derived from a different set of measurements. In fact, the measurement of the linear instantaneous *I-V* relationship helps validate the subtraction procedure used previously (Sanguinetti et al., 1995) to determine steady-state inactivation. This subtraction procedure assumed a linear instantaneous *I-V* relationship and calculated steady-state inactivation by taking the ratio of the experimentally determined steady-state current to the value of the predicted linear current. In contrast, h-*erg* has been reported to have an inwardly rectifying instantaneous *I-V* relationship that also contributes to steady-state rectification (Wang et al., 1996). However, under our conditions, the inward rectification of ferret I_{Kr} is entirely accounted for by a time-dependent inactivation process.

Models of the inactivation/rectification process of I_{Kr} have frequently treated inactivation as an independent process that is not coupled to activation. Our results suggest that coupling is necessary to explain the current transient observed at depolarized potentials and the voltage dependence of activation observed during the onset of a depolarizing pulse. It is not clear if this finding generalizes to I_{Kr} in other species. However, it is possible that coupling varies between species, with those species in which coupling is weak or absent showing no transient behavior at depolarized potentials.

The bell-shaped voltage dependence of inactivation time constants suggests a conventional single-step voltage-dependent inactivation mechanism. However, this provides us with little insight into underlying molecular mechanisms. It is difficult to reconcile the bell-shaped inactivation time constant curve with a conventional open channel blocker-type model. If voltage sensitivity resulted from permeation of a blocking particle into the pore, the on rate would be expected to be largely diffusion limited and therefore voltage insensitive, whereas the off rate would be expected to be voltage sensitive. If inactivation were to result from an N-type mechanism, similar voltage insensitivity of inactivation would also be predicted. Voltage dependence of either of these mechanisms could be conferred by open channel availability due to voltage-dependent activation (see Hille, 1992, for review). However, the voltage dependence of inactivation is weak compared with activation. Such a relationship suggests that the voltage dependence of inactivation does not arise from coupling to activation.

Thus, it seems likely that inactivation of ferret I_{Kr} has its own intrinsic voltage sensitivity, although the molecular basis for this sensitivity remains unknown.

Physiological consequences

The time and voltage dependence of currents is the determining factor in their physiological role in the regulation of action potential repolarization. Our study indicates two novel types of time- and voltage-dependent behavior of I_{Kr}. First, a transient outward current peak was observed during depolarization to positive potentials. Second, a slower time course of activation at positive potentials than previously suspected was established. Transient behavior of the E-4031-sensitive current in human atrial myocytes was evident in figure 1 *C* of Wang et al. (1994) for K^+ currents in human atrial myocytes, although the authors did not comment on this behavior. Studies of I_{Kr} in guinea pig or rabbit ventricular myocytes have not reported such transient behavior at positive potentials. This may be due to different species or experimental conditions. These conditions may have increased both the inactivation and activation kinetics of the drug-sensitive currents, to the point that the transient component was so small as to be unresolvable. Alternatively, the transient component of I_{Kr} may have been shifted to more hyperpolarized potentials (e.g., by $[Ca^{2+}]_o$ removal) than in previous studies (Sanguinetti and Jurkiewicz, 1992). Significantly, Inoue and Imanaga (1993) showed the existence of a transient K^+ current activated at positive potentials under experimental conditions that were similar to those employed in this study. Thus, the physiological significance of the transient component of I_{Kr} remains to be elucidated by studies that determine its dependence on temperature and ionic conditions. Nonetheless, our data suggest that I_{Kr} may contribute to the multiple components of the transient outward current (I_{to}) in some cardiac cell types (e.g., Coraboeuf and Carmeliet, 1982).

The differences between the apparent rate of macroscopic activation and the slower rate of activation of tail currents may predict a different degree of I_{Kr} activation during an action potential. It would therefore be of interest to compare the performance of this model with the formulation of Zeng et al. (1995) in a simulation of the cardiac action potential against the action potential data of Muraki et al. (1995). The activation rate of tail currents at -40 mV was compared with the activation rate of outward current at -10 mV in an envelope of tails test in guinea pig ventricular myocytes by Sanguinetti and Jurkiewicz (1990). The envelope of tails and the outward current were shown to correspond closely, suggesting that direct-fit analysis of the outward currents was an appropriate method for characterizing activation. Again, these differences between the guinea pig data and our data may reflect genuine differences in species or experimental conditions. However, as noted by Clay et al. (1995), the paradox concerning activation rate and steady-state inactivation is ubiquitous, despite species, tempera-

ture, or ionic conditions. Our data also suggest that distinguishing the rate of tail current activation from the rate of outward current activation at -10 mV would be difficult. The divergence between tail current and direct-fit measurements of activation are acutely sensitive to the test potential. For example, the rate of current activation analyzed from direct fit of outward current at $+10$ mV gave a time constant of activation of ~112 ms. Analysis of the tail currents indicates that activation at $+10$ mV occurs with a time constant of 230 ms. Thus, the differences in activation time-constant estimates may also reflect the potential range in which tail current activation was analyzed.

In conclusion, our data resolve the apparent paradox noted by Clay et al. (1995) concerning activation models of I_{Kr}. We propose that the apparent paradox arises from the overlap of inactivation and activation of I_{Kr}, which renders conventional analysis of activation characteristics invalid at depolarized potentials. Although steady-state activation measured from tail currents is insensitive to inactivation, the apparent rate constants of activation and deactivation are shifted to more negative potentials due to overlap and coupling with inactivation. This overlap also masks non-Hodgkin-Huxley (1952)-like properties of I_{Kr}, such as voltage-dependent saturation of the activation rate. The voltage-dependent saturation of activation rate may be of significant physiological consequence in determining the total contribution of I_{Kr} to the action potential plateau.

REFERENCES

Aldrich, R. W., D. P. Corey, and C. F. Stevens. 1983. A reinterpretation of mammalian sodium channel gating based on single channel recording. *Nature.* 306:436–441.

Aldrich, R. W., and C. F. Stevens. 1987. Voltage dependent gating of single sodium channels from mammalian neuroblastoma cells. *J. Neurosci.* 7:418–431.

Anumonwo, J. M. B., L. C. Freeman, W. M. Kwok, and R. S. Kass. 1992. Delayed rectification in single cells isolated from guinea pig sinoatrial node. *Am. J. Physiol.* 262:H921–H925.

Apkon, M., and J. M. Nerbonne. 1991. Characterization of two distinct depolarization-activated K$^+$ currents in isolated rat ventricular myocytes. *J. Gen. Physiol.* 97:973–1011.

Armstrong, C. M. 1966. Time course of TEA$^+$ induced anomalous rectification in squid giant axons. *J. Gen. Physiol.* 50:491–503.

Backx, P. M., and E. Marban. 1993. Background potassium current active during the plateau of the action potential in guinea pig ventricular myocytes. *Circ. Res.* 72:890–900.

Balser, J. R., P. B. Bennett, and D. M. Roden. 1990. Time-dependent outward current in guinea pig ventricular myocytes. *J. Gen. Physiol.* 96:835–863.

Beuckelmann, D. J., M. Näbauer, and E. Erdmann. 1993. Alterations of K$^+$ currents in isolated human ventricular myocytes from patients with terminal heart failure. *Circ. Res.* 73:379–385.

Campbell, D. L., R. L. Rasmusson, Y. Qu, and H. C. Strauss. 1993. The calcium-independent transient outward potassium current in isolated ferret right ventricular myocytes. *J. Gen. Physiol.* 101:571–601.

Campbell, D. L., R. L. Rasmusson, and H. C. Strauss. 1992. Ionic current mechanisms generating vertebrate primary pacemaker activity at the single cell level: an integrative view. *Annu. Rev. Physiol.* 54:279–302.

Carmeliet, E. 1992. Voltage- and time-dependent block of the delayed K$^+$ current in cardiac myocytes by dofetilide. *J. Pharmacol. Exp. Ther.* 262:809–817.

Carmeliet, E. 1993. Use-dependent block and use-dependent unblock of delayed rectifier K$^+$ current by amokalant in rabbit ventricular myocytes. *Circ. Res.* 73:857–868.

Castellino, R. C., M. J. Morales, H. C. Strauss, and R. L. Rasmusson. 1995. Time- and voltage-dependent modulation of a Kv1.4 channel by a β-subunit (Kvβ3) cloned from ferret ventricle. *Am. J. Physiol.* 269(*Heart Circ. Physiol.* 38):H385–H391.

Clay, J. R., A. Ogbaghebriel, T. Paquette, B. I. Sasyniuk, and A. Shrier. 1995. A quantitative description of the E-4031 sensitive repolarization current in rabbit ventricular myocytes. *Biophys. J.* 69:1830–1837.

Cole, K. S., and J. W. Moore. 1960. Potassium ion current in the squid giant axon. Dynamic characteristics. *Biophys. J.* 1:1–14.

Coraboeuf, E., and E. Carmeliet. 1982. Existence of two transient outward currents in sheep Purkinje fibers. *Pflugers Arch.* 392:352–359.

Curran, M. E., I. Splawski, K. W. Timothy, G. M. Vincent, E. D. Green, and M. T. Keating. 1995. A molecular basis for cardiac arrhythmia: HERG mutations cause long QT syndrome. *Cell.* 80:795–803.

DiFrancesco, D. 1985. The cardiac hyperpolarizing-activated current, I_f. Origins and developments. *Prog. Biophys. Mol. Biol.* 46:163–183.

Fedida, D., B. Wible, Z. Wang, B. Fermini, F. Faust, S. Nattel, and A. M. Brown. 1993. Identity of a novel delayed rectifier current from human heart with a cloned K$^+$ channel current. *Circ. Res.* 73:210–216.

Hille, B. 1992. Ionic Channels of Excitable Membranes, 2nd ed. Sinauer Associates, Sunderland, MA.

Hodgkin, A. L., and A. F. Huxley. 1952. A quantitative description of membrane current and its application to conduction and excitation in nerve. *J. Physiol.* 117:500–544.

Hoshi, T., W. N. Zaggotta, and R. W. Aldrich. 1990. Biophysical and molecular mechanisms of *Shaker* potassium channel inactivation. *Science.* 250:533–538.

Inoue, M., and I. Imanaga. 1993. Masking of an A-type K$^+$ channel in guinea pig by extracellular Ca^{2+}. *Am. J. Physiol.* 264:C1434–C1438.

Jurkiewicz, N. K., and M. C. Sanguinetti. 1993. Rate dependent prolongation of cardiac action potentials by a methanesulfanilide agent. Specific block of rapidly activating delayed rectifier K$^+$ current by dofetilide. *Circ. Res.* 72:75–83.

Kass, R. S. 1995. Delayed potassium channels in the heart: cellular, molecular, and regulatory properties. *In* Cardiac Electrophysiology: From Cell to Bedside, 2nd ed. D. P. Zipes and J. Jalife, editors. W. B. Saunders, Philadelphia. 74–82.

Liu, S., R. L. Rasmusson, D. L. Campbell, S. Wang, and H. C. Strauss. 1996. Activation and inactivation kinetics of an E-4031 sensitive current (I_{Kr}) from single ferret atrial myocytes. *Biophys. J.* 70:A399.

McAllister, R. E., D. Noble, and R. W. Tsien. 1975. Reconstruction of the electrical activity of cardiac Purkinje fibers. *J. Physiol. (Lond.).* 251: 1–59.

Muraki, K., Y. Imaizumi, M. Watanabe, Y. Habuchi, and W. R. Giles. 1995. Delayed rectifier K+ current in rabbit atrial muscle. *Am. J. Physiol.* 269(*Heart Circ. Physiol.* 38):H524–H532.

Noble, D. 1984. The surprising heart: a review of recent progress in cardiac electrophysiology. *J. Physiol. (Lond.).* 353:1–50.

Noble, D., and R. W. Tsien. 1968. The kinetics and rectifier properties of the slow potassium current in cardiac Purkinje fibers. *J. Physiol. (Lond.).* 195:185–214.

Noble, D., and R. W. Tsien. 1969. Outward membrane currents activated in the plateau range of potentials in cardiac Purkinje fibers. *J. Physiol. (Lond.).* 200:205–231.

Sanguinetti, M. C., C. Jiang, M. E. Curran, and M. T. Keating. 1995. A mechanistic link between an inherited and an acquired cardiac arrhythmia: HERG encodes the I_{Kr} potassium channel. *Cell.* 81: 299–307.

Sanguinetti, M. C., and N. K. Jurkiewicz. 1990. Two components of cardiac delayed rectifier K^+ current. Differential sensitivity to block by class III antiarrhythmic agents. *J. Gen. Physiol.* 96:195–215.

Sanguinetti, M. C., and N. K. Jurkiewicz. 1991. Delayed rectifier outward K^+ current is composed of two currents in guinea pig atrial cells. *Am. J. Physiol.* 260:H393–H399.

Sanguinetti, M. C., and N. K. Jurkiewicz. 1992. Role of external Ca^{2+} and K^+ in gating of cardiac delayed rectifier K^+ currents. *Pflügers Arch.* 420:180–186.

Shibasaki, T. 1987. Conductance and kinetics of delayed rectifier potassium channels in nodal cells of the rabbit heart. *J. Physiol. (Lond.).* 387:227–250.

Shibata, E. F., and W. R. Giles. 1985. Ionic currents which generate the spontaneous diastolic depolarizations in individual cardiac pacemaker cells. *Proc. Natl. Acad. Sci. USA.* 82:7796–7800.

Snyders, D. J., M. M. Tamkun, and P. B. Bennett. 1993. A rapidly activating and slowly inactivating potassium channel cloned from human heart. *J. Gen. Physiol.* 101:513–543.

Trudeau, M. C., J. W. Warmke, B. Ganetzky, and G. A. Robertson. 1995. HERG, a human inward rectifier in the voltage-gated potassium channel family. *Science.* 269:92–95.

Verheijck, E. E., A. C. G. van Ginneken, J. Bourier, and L. N. Bouman. 1995. Effects of delayed rectifier current blockade by E-4031 on impulse generation in single sinoatrial nodal myocytes of the rabbit. *Circ. Res.* 76:607–615.

Wang, Q., B. Fermini, and S. Nattel. 1993. Delayed rectifier outward current and repolarization in human atrial myocytes. *Circ. Res.* 73: 276–285.

Wang, S., M. J. Morales, S. Liu, H. C. Strauss, and R. L. Rasmusson. 1996. Instantaneous and time-dependent components of rectification of h-*erg* expressed in *Xenopus* oocytes. *Biophys. J.* 70:A312.

Wang, Z., B. Fermini, and S. Nattel. 1994. Rapid and slow components of delayed rectifier current in human atrial myocytes. *Cardiovasc. Res.* 28:1540–1546.

Zaggotta, W. N., and R. W. Aldrich. 1990. Voltage-dependent gating of *Shaker* A-type potassium channels in *Drosophila* muscle. *J. Gen. Physiol.* 95:25–60.

Zeng, J., K. R. Laurita, D. S. Rosenbaum, and Y. Rudy. 1995. Two components of the delayed rectifier K^+ current in ventricular myocytes of the guinea pig type. *Circ. Res.* 77:140–152.